Journal of
Applied Crystallography
ISSN 0021-8898

Received 27 March 2000
Accepted 26 June 2000

© 2000 International Union of Crystallography
Printed in Great Britain – all rights reserved

Microcrystallography with an X-ray waveguide

M. Müller,[a] M. Burghammer,[a] D. Flot,[a] C. Riekel,[a]* C. Morawe,[a] B. Murphy[b] and A. Cedola[c]

[a]European Synchrotron Radiation Facility, BP 220, F-38043 Grenoble CEDEX, France, [b]CLRC Daresbury Laboratory, Warrington, Cheshire WA4 4AD, England, and [c]Istituto di Elettronica dello Stato Solido Via Cineto Romano 42, 00156 Roma, Italy. Correspondence e-mail: riekel@esrf.fr

A waveguide microdiffraction setup is described for an undulator beamline at the European Synchrotron Radiation Facility. The composite optics consists of a waveguide, which confines the beam vertically, and a horizontally focusing multilayer mirror. A beam size of about 0.1 × 3 μm (vertical × horizontal) at λ = 0.095 nm has been obtained. The sample stage comprises a three-axis gantry with micrometre precision and a three-axis piezo-scanner with about 0.1 μm repeatability. Diffraction experiments are demonstrated for selected inorganic and polymeric samples. Possibilities for scanning diffractometry and small-angle scattering experiments are discussed.

1. Introduction

X-ray microdiffraction experiments based on third-generation synchrotron radiation sources are routinely performed on the 1 μm scale (Riekel, 2000). There is increasing interest in submicrometre beam sizes in order to investigate structural organization on mesoscopic length scales. Submicrometre X-ray beams can be obtained by a variety of optical elements based on total reflection, diffraction or refraction (Table 1).

X-ray waveguides have been shown to provide beams of about 0.1 μm size in one direction (Cedola *et al.*, 1998). Radiation transport occurs through a light element layer (typically carbon) by total reflection at opposing metallic layers (Spiller & Segmüller, 1974). X-ray waveguides based on parallel plates with an air gap have also been reported (Zwanenburg *et al.*, 1999). The transport is limited to a number of modes where standing-wave patterns are generated (Feng *et al.*, 1995; Jark *et al.*, 1996). Because of the linear polarization of synchrotron radiation, the electric field of the incoming beam and of the reflected beams stays normal to the incidence plane. Only the transverse electric (TE) modes therefore propagate.

Interest in these optical elements is linked to the unique combination of small beam size, coherent radiation output and use in the hard X-ray regime. Research and development of waveguides has principally been performed at synchrotron radiation sources and in particular at third-generation synchrotron radiation sources (Feng *et al.*, 1995; Jark *et al.*, 1996; Lagomarsino *et al.*, 1997; Cedola *et al.*, 1998). To date, emphasis has been placed on exploiting the coherent radiation for imaging (Lagomarsino *et al.*, 1997) and diffraction (DiFonzo *et al.*, 2000). In these experiments, vertical magnification (M) is defined by $M = (z_1 + z_2)/z_1$, where z_1 is the sample-to-waveguide exit distance and z_2 is the sample-to-detector distance. By contrast, the present article will concentrate on diffraction experiments in which the primary interest is in an X-ray beam that is as small as possible at the sample position. A further aim of this work was to increase the flux density of the waveguide setup for the study of small and weakly scattering samples (*e.g.* fibres) by adding a horizontally focusing mirror and to develop a practical approach to sample alignment and scanning.

The article is organized as follows: §2 describes the instrumentation; §3 reports on the performance of the system; selected applications are described in §4; in §5 the mid-term development potential of X-ray waveguides is discussed.

2. Instrumentation

The production and characterization of X-ray waveguides has been described elsewhere (Jark *et al.*, 1996; Lagomarsino *et al.*, 1997; Cedola *et al.*, 1998). The waveguide used in the present study had an Mo/C/Mo sandwich structure with a carbon layer of thickness ∼80 nm. The waveguide structure was deposited on an ultrasmooth silicon substrate by sputtering techniques, at the multilayer laboratory of Sincrotrone Trieste (Jark *et al.*, 1996). It was attached to a special support structure. Details will be published elsewhere (Jark *et al.*, 2000).

Experiments were performed at the ESRF microfocus beamline at a wavelength, λ, of 0.0948 nm [Si(111) double-crystal monochromator] during a 16 bunch filling period with ≤70 mA ring current. A setup combining the waveguide with a horizontally focusing mirror and a sample scanning stage was developed. The standard ellipsoidal mirror was moved out of the beam (Riekel, 2000). The setup is shown schematically in Fig. 1. Mechanical elements, including the waveguide, were fixed to a rigid frame. Apart from the piezo-scanning stage, motions were based on standard stepping-motor modules (Owis, ESRF proprietary and Huber). The waveguide was at 34 m from the low-β undulator source. The setup was installed on a 'breadboard', which was placed on a hexapod support

Table 1
Overview of reported submicrometre beam sizes obtained by selected X-ray optics.

Beam size is usually indicated by the full width at half-maximum (FWHM). The waveguide optics source point has an FWHM size of half of the resonator thickness (Jark *et al.*, 1996).

Optical system	Size (μm)	Comments	Reference
Mirror	0.7		Iida & Hirano (1996), Padmore *et al.* (1997)
Waveguide	∼0.1	One-dimensional	Feng *et al.* (1995), Jark *et al.* (1996)
Glass capillary	0.09	Pink beam	Bilderback *et al.* (1994)
Fresnel optics	0.15	<0.09 third order	Lai *et al.* (1998)
Bragg–Fresnel optics	0.8	One-dimensional	Kuznetsov *et al.* (1994)
Refractive lens	0.3		Snigirev (personal communication), Snigirev *et al.* (1996)

structure. This allows easy alignment of the setup in the beam. In order to increase the flux density and confine the beam horizontally, a laterally graded multilayer mirror was used. The waveguide was attached to a Physics Instruments rotation stage (WR_y) and could be translated vertically and horizontally (WT_z, WT_y). The sample scanning stage provided a three-axis gantry (ST_x, ST_y, ST_z) for transfer of the sample between a horizontal microscope, with a charge-coupled device (CCD) camera, and the beam (∼1 μm repeatability). A similar approach had already been used for a glass-capillary scanning setup (Riekel, 2000). A second stage comprising a 360° rotation axis (SR_z), two motorized arcs for sample alignment (SR_x, SR_y; ±20°) and a three-dimensional piezo-scanner with about 70 μm stroke and about 0.1 μm repeatability for each axis (Piezo-Jena; SP_x, SP_y, SP_z) was placed on top of the basic gantry. An inductive gauge was used to verify the positioning and repeatability of the piezo-scanner. An additional microscope, enabling one to look down onto the waveguide at the beam exit, was used to position the sample close to the waveguide. Once the sample was roughly aligned, further displacements were made with the piezo-scanner.

A laterally graded multilayer mirror served for horizontal focusing (Morawe *et al.*, 1999). The mirror was designed to be used either at 13 keV or 20 keV without changing the focal distance (400 mm). Two different B_4C/Ru coatings were used. For the present experiment, only the coating optimized for 13 keV was used. This coating consisted of 70 double layers of about 4.0 nm thickness on a superpolished silica substrate. It was grown in the ESRF multilayer laboratory (Morawe *et al.*, 1999). The full vertical beam size (∼0.8 mm) could be accepted although the waveguide restricts the vertical acceptance to ∼50 μm. The mirror was aspherically bent by a bender with New Focus piezo screw elements (Ziegler *et al.*, 1996). It could be positioned by horizontal and vertical translations (MT_y, MT_z) and rotation around the vertical axis (MR_z). The reflectivity at 13 keV was about 0.85.

The setup was installed in a thermostatically controlled hutch (298 ± 0.5 K) with the temperature sensor close to the setup. The long-term temperature stability at the sample position was not, however, monitored.

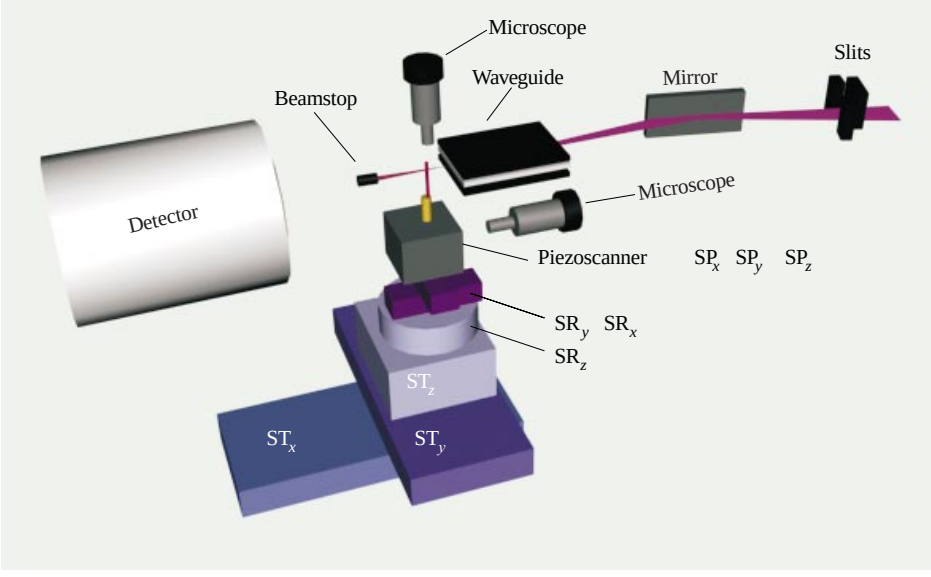

Figure 1
Schematic of the waveguide setup. Note the coordinate system with x along the beam direction, y transverse and z vertical. Only the movements of the sample stage are indicated.

3. System performance

3.1. Alignment and flux

The shape of the mirror was optimized by step scanning a fine slit in front of the mirror, horizontally across the surface, and recording at every step the reflected beam using a high-resolution CCD camera with X-ray converter (Hignette *et al.*, 1997). From this, a wavefront error of 3.3 μrad FWHM (full width at half-maximum) was derived (Hignette *et al.*, 1997). This allows the prediction of a spot size of 2.9 μm FWHM by ray tracing. The size of the horizontal spot was then determined experimentally as a function of the distance from the mirror by knife-edge scans using an aperture, of hole diameter 20 μm (2 mm diameter × 0.6 mm; Pt–Ir; Pella Inc.), and a photodiode detector. Fig. 2(*a*) shows a typical knife-edge scan at the ideal position

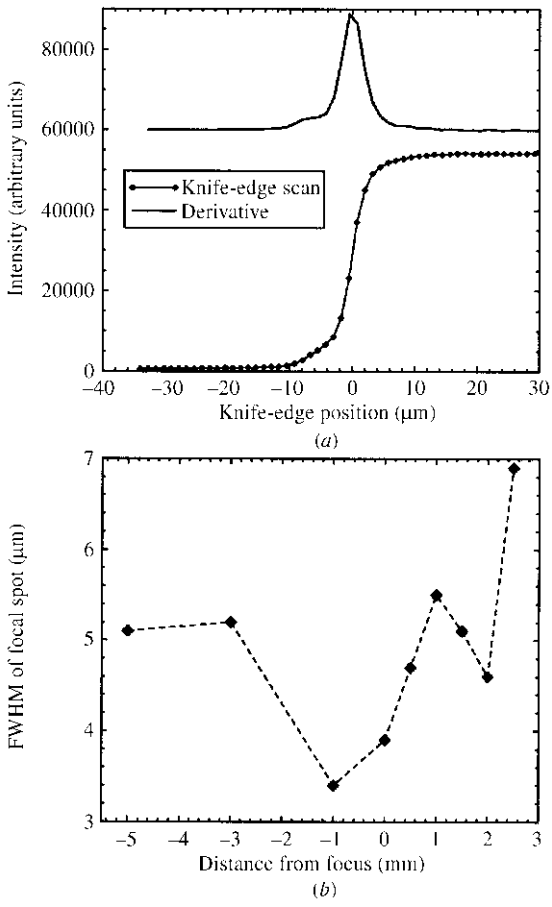

Figure 2
(*a*) Knife-edge scan of the horizontal beam size and its derivative. A value of 3.9 μm FWHM is derived from this scan. (*b*) Variation of horizontal beam size (FWHM) as a function of relative distance to the centre of the mirror (400 mm absolute distance).

(400 mm from middle of mirror) and its derivative, which results in a focus size of 3.9 μm FWHM. Fig. 2(*b*) shows the variation of the spot size as a function of the relative distance from the focus. The minimum corresponds to about 3.4 μm FWHM and remains rather constant within about 1 mm. Convolution of the slope-error dependent 2.9 μm FWHM with the demagnified source size of 1.6 μm FWHM (see below) results in 3.3 μm FWHM, which is in good agreement with the observed value.

The mirror accepted about 1.7 mm horizontally from the full 6 mm of monochromatic beam. The waveguide was aligned using an assembly of a horizontal entrance slit, a transparent photodiode and a high-resolution CCD camera. The slit could be scanned vertically across the beam profile in order to separate the totally reflected and waveguided beams from the direct beam. For subsequent experiments, the TE_0 mode was used. The beam was defined horizontally and vertically by a slit system, which was located upstream from the mirror in order to reduce background scattering from the waveguide. Additional lead shielding of the beam path between the mirror and the waveguide was required. The total air path upstream from the waveguide was about 1 m. A flux of 2×10^8 photons s^{-1} corresponding to a flux density of 10^7 photons s^{-1} mA^{-1} μm^{-2} for a nominally 0.1×3 μm beam was determined for a machine current of 70 mA by the photodiode. The setup proved to be quite stable, even after several days of operation. The vertical position of the waveguide had to be realigned every few hours. This misalignment might be caused by the relative motion between the last defining slits located in the upstream optical hutch and the waveguide setup. For further diffraction experiments, a MAR CCD detector with an entrance window of 130 mm diameter and $(2048)^2$ pixels was used. The pixel size was 64.45×64.45 μm. The cooled detector (173 K) was read out with 16 bits. Data were analysed using the software package *FIT2D* (Hammersley, http://www.esrf.fr/computing/expg/subgroups/data_analysis/FIT2D/index.html).

3.2. Beam parameters

The source parameters of the low-β undulator at 13 keV are: $s_x = 134$, $s_z = 24$ μm FWHM; $s'_x = 208$, $s'_z = 21$ μrad FWHM (x horizontal, z vertical). The horizontal beam acceptance of 1.7 mm by the mirror corresponds to a horizontal beam divergence of about 25 μrad. Demagnification by a factor of 84 will increase the horizontal divergence at the focus to about 4.9 mrad, while the vertical divergence at the exit of the waveguide is about 1 mrad for the two convoluted branches of the TE_0 mode.

The vertical beam profile of the TE_0 (first order) mode in the far-field approximation has been simulated by a Gaussian beam (Jark *et al.*, 1996; Cedola, 1998). The present Fraunhofer diffraction pattern at a distance of 496.2 mm from the waveguide exit shows at least three orders (Fig. 3). Reflectivity measurements on the same waveguide indicate a thickness of 75 nm FWHM at the waveguide exit (Jark *et al.*, 2000). In addition, the Fraunhofer pattern is modulated by fringes. The fringes might be caused by irregularities at the edge of the silicon/waveguide interface, which result in slight path differences between different portions of the outgoing beam. The horizontal profile of the first secondary maximum ($s \simeq 0.22$ nm^{-1}) can be fitted by a Gaussian function. The width of 2.25 mm (FWHM) is related to the horizontal beam divergence. The expected beam size in the horizontal direction, b_x, can be derived from

$$b_x = [x^2 + (x'L)^2]^{1/2}, \quad (1)$$

where x is the beam size at the exit of the waveguide, x' is the divergence of the beam and L is the waveguide-to-detector distance. With the parameters $x = 0.003$ mm, $x' = 4.9$ mrad and $L = 496.2$ mm, it follows that $b_x \simeq x'L$ and $b_x = 2.24$ mm (FWHM), which is in good agreement with the calculated value.

4. Diffraction experiments

Applications presented in this section have been selected principally to demonstrate the experimental possibilities; in-depth analysis has not been attempted.

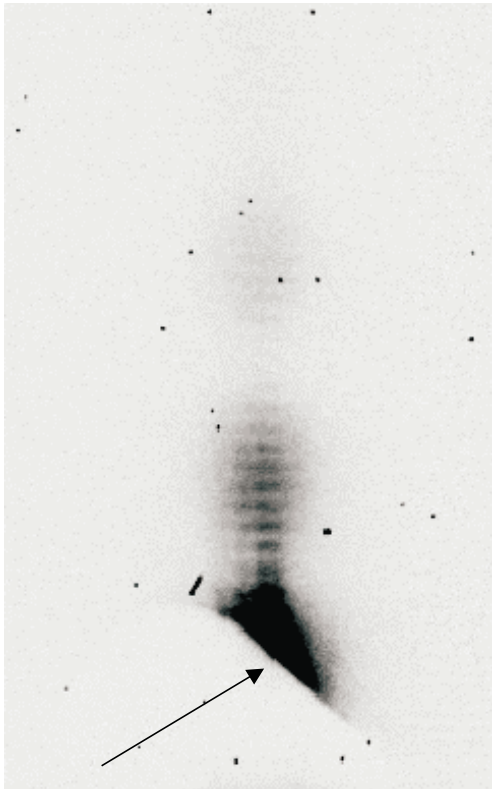

Figure 3
Fraunhofer diffraction pattern observed with the CCD detector at 496.2 mm from the waveguide exit. The distance was calibrated using an Al_2O_3 standard. A beamstop covers the direct beam.

4.1. Practical aspects

The vertical divergence of about 1 mrad of the TE_0 mode necessitates approaching the sample sufficiently close to the waveguide to obtain the smallest vertical beam size possible. The broadening in the vertical direction, Δ_z, can be approximated by (Cedola, 1998)

$$\Delta_z = (\lambda x)^{1/2}. \quad (2)$$

At $\lambda = 0.095$ nm the sample should be within $x = 100$ µm from the exit of the waveguide in order to limit Δ_z to 0.1 µm. This is feasible for transmission experiments provided that the sample thickness is sufficiently small. The microscope enabling one to look down on the waveguide exit can be used to determine this distance accurately. Fig. 4 shows a grain of Al_2O_3 powder on a glass tip at about 150 µm from the waveguide exit. As the samples discussed below were always less than 1 mm from the exit of the waveguide, one can also assume that the horizontal focal spot was close to 3 µm (Fig. 2*b*).

4.2. Beam size effects

Experiments described below concern samples with a large number of scattering objects. Comparing the beam size (S) with the size of the coherently scattering object (L) allows a rough classification of the expected scattering pattern. Thus for $L \simeq S$, one expects the presence of spikes on the Debye–Scherrer rings, while a continuous intensity distribution is expected for $L < S$.

$L \simeq S$ applies to Al_2O_3 powder [α-Al_2O_3; Standard Reference Material 674a, National Bureau of Standards (NBS)] which consists of crystallites with hexagonal habit with a basal plane diameter of $\geq$0.1 µm. This corresponds roughly to the area of the beam, *i.e.* about 0.3 µm^2 (Fig. 5*a*). The diffraction pattern from the Al_2O_3 grain (transformed to polar coordinates) shows that the intensity distribution of each reflection is composed of spikes as a result of the sampling of individual crystallites by a beam of about 0.3 µm^2 within a sample depth of about 100 µm (Figs. 5*b* and 5*c*). This can be seen in more detail for the $2\bar{1}0$ reflection in Fig. 5(*c*).

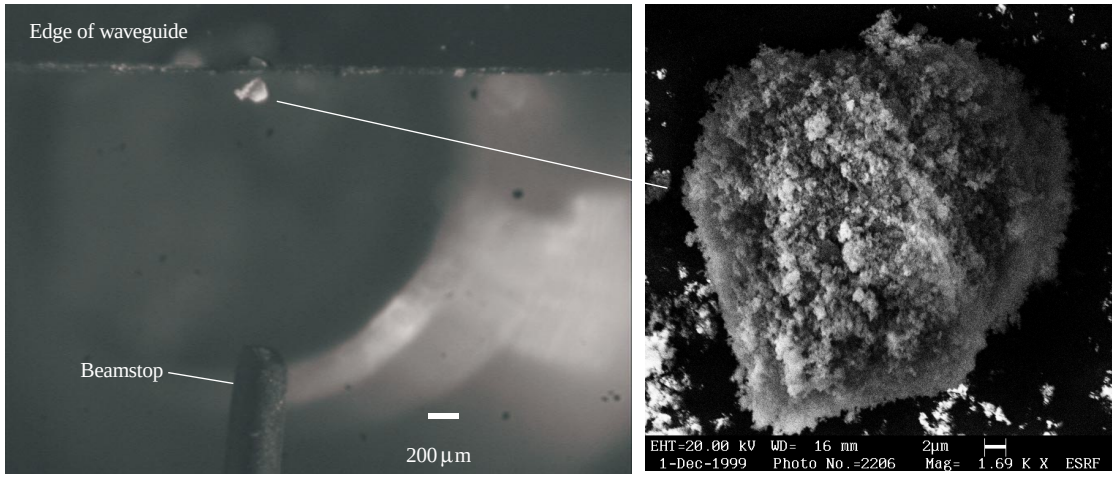

Figure 4
Top view of the waveguide exit with an Al_2O_3 powder grain on a glass fibre. The scanning electron microscopy (SEM) image shows a magnified view of the speck.

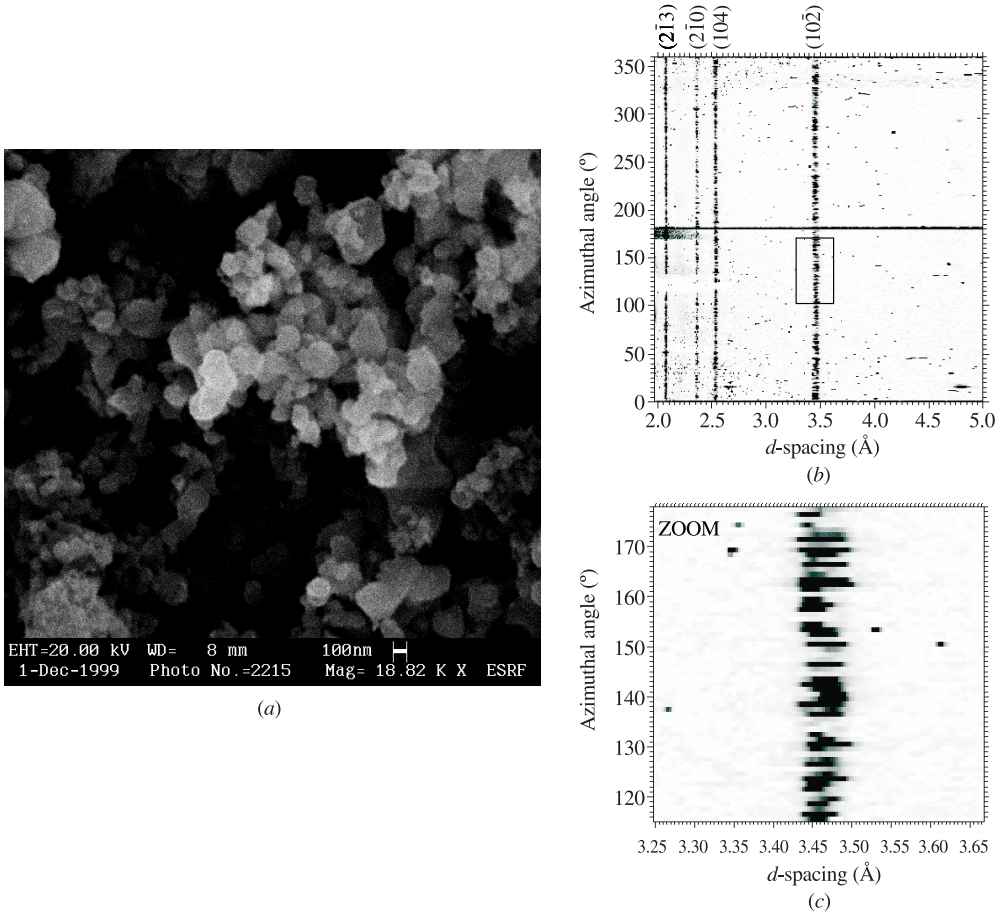

Figure 5
(*a*) SEM images of crystallites in an Al_2O_3 powder grain. The vertical dimension of the X-ray beam corresponds to the scale-bar. (*b*) Corresponding X-ray diffraction pattern in polar coordinates recorded in 180 s with the waveguide beam, and azimuthally regrouped. Sample-to-detector distance: 113.8 mm. (*c*) An enlarged portion of the 10$\bar{2}$ reflection.

A grain from the handle of a Koan transport amphora (used in the period 300 BC to 100 AD) shows a complex phase mixture, which is typical for ceramic samples. The scanning electron microscopy (SEM) image (Fig. 6*a*) suggests compositional changes on different length scales. Correspondingly, the diffraction pattern (transformed to polar coordinates; Fig. 6*b*) shows that the size of coherently scattering objects varies considerably. One recognizes again spikes indicating scattering objects corresponding to $L \simeq S$. Weaker continuous lines below the spikes suggest the presence of smaller domains (fine powders) with $L < S$. In addition, reflections arising from large ($L > S$) single-crystalline domains are present. An averaged powder pattern was obtained by azimuthal integration of the two-dimensional pattern (Fig. 6*c*, red line). It differs considerably from a second pattern recorded at a distance of 17 µm (Fig. 6*c*, blue line). The line intensities suggest differences in the relative amount and/or texture of the components. The calculated positions of reflections suggest the presence of magnesian calcite, diopside and quartz. The first (red) diffraction diagram (Fig. 6*c*) is dominated by the strong 101 quartz reflection. It is clearly visible as a prominent single-crystal reflection (Figs. 6*b* and 6*d*). The second strong reflection with several maxima at different *d*-spacings corresponds to a presently unidentified component. The present data demonstrate that with submicrometre beam sizes, the signals from weak phases can be detected and discriminated from the strong contributions of quartz or calcites.

$L < S$ applies to hierarchically organized polymers, which are often composed of nanometre-sized coherently scattering domains (Sawyer & Grubb, 1996). In the case of polymer fibres, a fibre diffraction pattern is therefore expected. This is the case for a single fibre of poly(*p*-phenylene terephthalamide) (PPTA; trade name Kevlar[49]; obtained from Goodfellow). The pattern from the centre of a fibre of ∼11 µm diameter (Fig. 7) is identical to patterns obtained with a 3 µm beam (Riekel *et al.*, 1999). The distance to the waveguide exit was <0.1 mm. The fibre was rotated by $\Delta SR_x = 5^\circ$ in order to separate the equatorial pattern from the background of the waveguide. The asymmetry of the meridional pattern suggests that the fibre axis was not completely normal to the beam direction. For this weak scattering pattern, residual background from the shielding material is visible. The best fit of the equatorial profiles of the 110/200 reflections can be obtained with two Voigtian functions and a first-order polynomial background. Using the Al_2O_3 standard as a reference material (see below) and the Scherrer formula, one obtains average particle size (L_{hkl}) values of $L_{110} = 8.5$ nm and $L_{200} = 6.2$ nm.

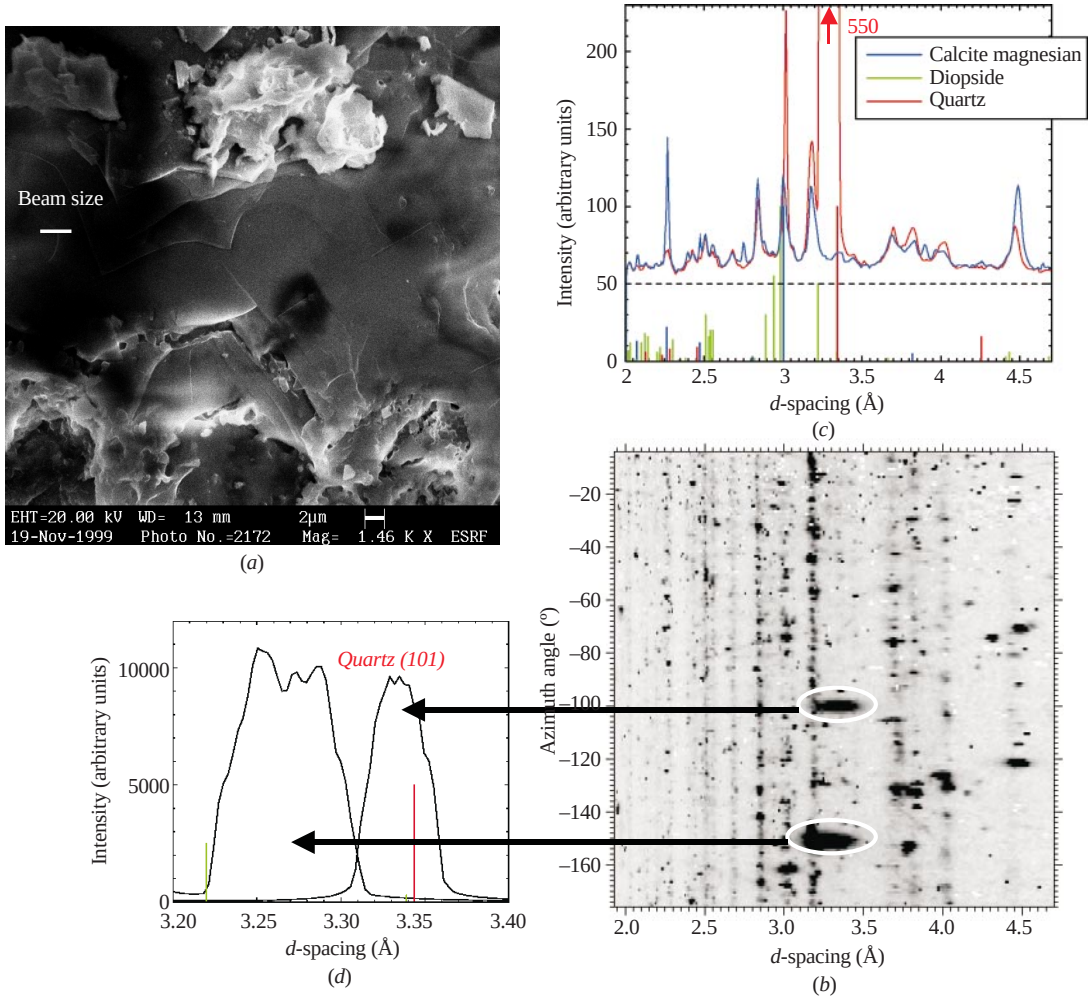

Figure 6
Results for a sample of an ancient ceramic (handle of a Koan transport amphora). (*a*) SEM image of a powder grain. (*b*) Diffraction pattern of a similar grain in polar coordinates. The measuring time was 120 s. The intensity was cut at 10% of the maximum intensity to enhance the visibility of weak reflections. The spread in *d*-spacings of the two strongest reflections is shown quantitatively in (*d*). (*c*) One-dimensional powder patterns obtained by integration along the azimuth. The red curve corresponds to the two-dimensional pattern in (*b*); the blue one was recorded at a distance of 17 µm. The calculated line patterns of magnesian calcite (blue bars), diopside (green bars) and quartz (red bars) are shown. (*d*) Detail of two single spots in (*b*). The red bar corresponds to the position of the quartz 101 reflection.

Synchrotron radiation experiments on a Kevlar[49] fibre bundle are in good agreement, with L_{110} = 7.2 nm and L_{200} = 6.0 nm (Jackson *et al.*, 1994).

4.3. Submicrometre scanning diffractometry

Scanning X-ray diffractometry is an *in situ* technique, which compliments electron diffraction techniques, the latter requiring thin sections and a vacuum (Riekel, 2000). The anisotropy of the present microbeam suggests using one-dimensional scans in the vertical direction in order to obtain the highest positional resolution. This is of particular interest for special geometries, such as those of fibres or interfaces. The dimension of a single PPTA (Kevlar[49]) fibre and the dimensions of the beam are shown in Fig. 8(*a*). The piezo-scanner was used for the line scan. Fig. 8(*b*) shows the *d*-spacing variations of the 110/200 reflections during a linear scan along the centre of the fibre with ΔSP_z = 0.08 µm steps. After every step, a 180 s diffraction pattern was recorded. Fig. 9 shows the variation of the azimuthal width (FWHM) of the 110 and 200 reflections. A Gaussian function appears to be a good approximation to the azimuthal profile as shown in Fig. 9. The average width corresponds closely to that observed with an S = 3 µm beam for a different Kevlar[49] fibre (Riekel *et al.*, 1999), also with respect to the slightly larger width of the 110 reflection as compared to the 200 reflection. The lines correspond to a least-squares fit to the data. Whether or not the different slopes imply, in practice, the existence of a local inversion of the broadening, cannot be stated without a larger scan range.

The principal PPTA allomorph has a monoclinic (pseudo-orthorhombic) unit cell (Northolt, 1974). The polymer chains form hydrogen-bonded sheets, which show a radial organization around the fibre axis (Dobb *et al.*, 1977). Electron scattering experiments on Kevlar sections suggest that these sheets form pleats along the fibre axis with a periodicity of

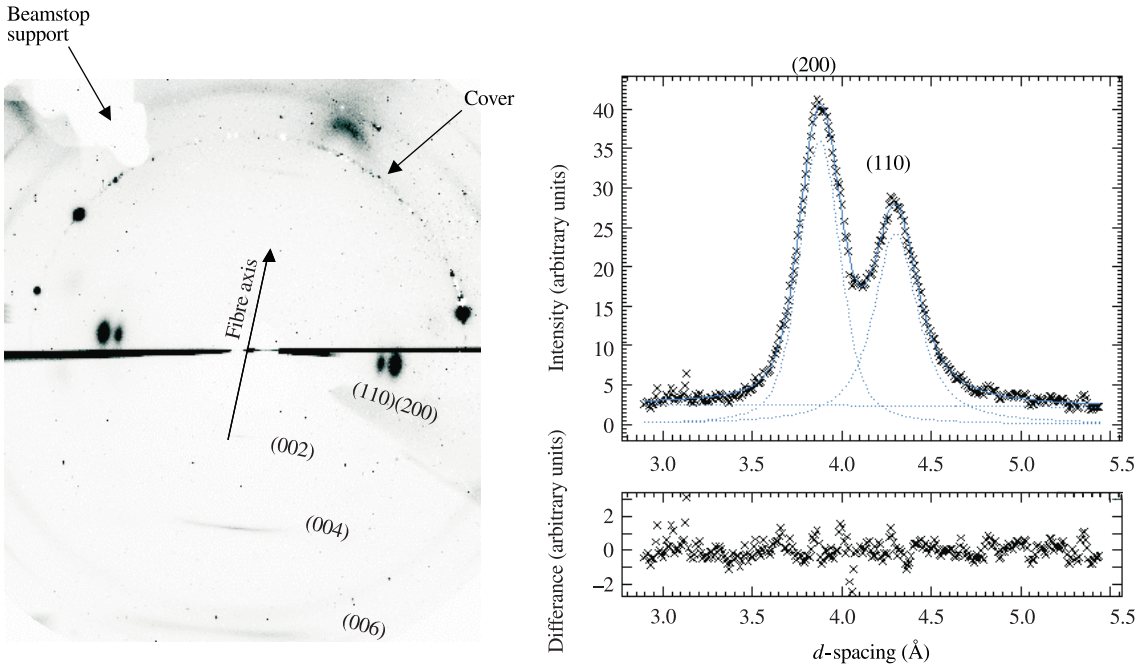

Figure 7
WAXS pattern obtained from a single Kevlar[49] fibre, supported on a glass tip. The pattern corresponds to the average of 21 patterns obtained during a line scan (Fig. 8). The horizontal stripe is caused by the background scattering, as in Fig. 5. Inhomogeneous background scattering is mainly the result of scattering from the cover plate (Bragg ring and spots on the ring) and the lack of local shielding. The radial profile of the two equatorial reflections from a single pattern has been fitted by two Voigtian functions and a first-order polynomial background.

0.5 µm and an angle of 170° between neighbouring pleats (Dobb *et al.*, 1977). For a homogeneous and regular pleat distribution throughout the fibre, one would expect to observe a modulation of the azimuthal width of meridional reflections in an X-ray transmission experiment on a single fibre. Thus, the orientation of crystalline blocks should reflect the pleat distribution. The fibre axis implies a rotational averaging of blocks for every position along the fibre. The local azimuthal width of meridional reflections thus reflects the local orientation distribution of blocks along the fibre axis. A slight modulation is indeed observed for the 004 reflection, as shown in Figs. 10(*a*) and 10(*b*). The minima correspond to slightly

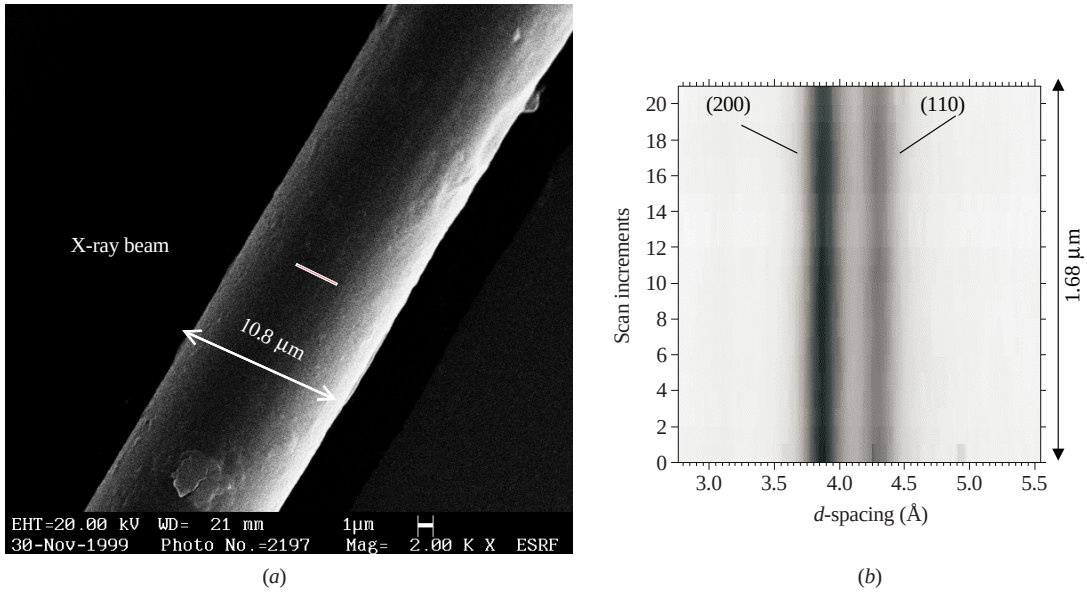

(*a*) (*b*)

Figure 8
(*a*) SEM image of a Kevlar[49] fibre. The size of the X-ray beam is indicated within the fibre. (*b*) *d*-spacing variation of the 110/200 reflections for a linear scan along the centre of the fibre, with 21 steps and a 0.08 µm step increment.

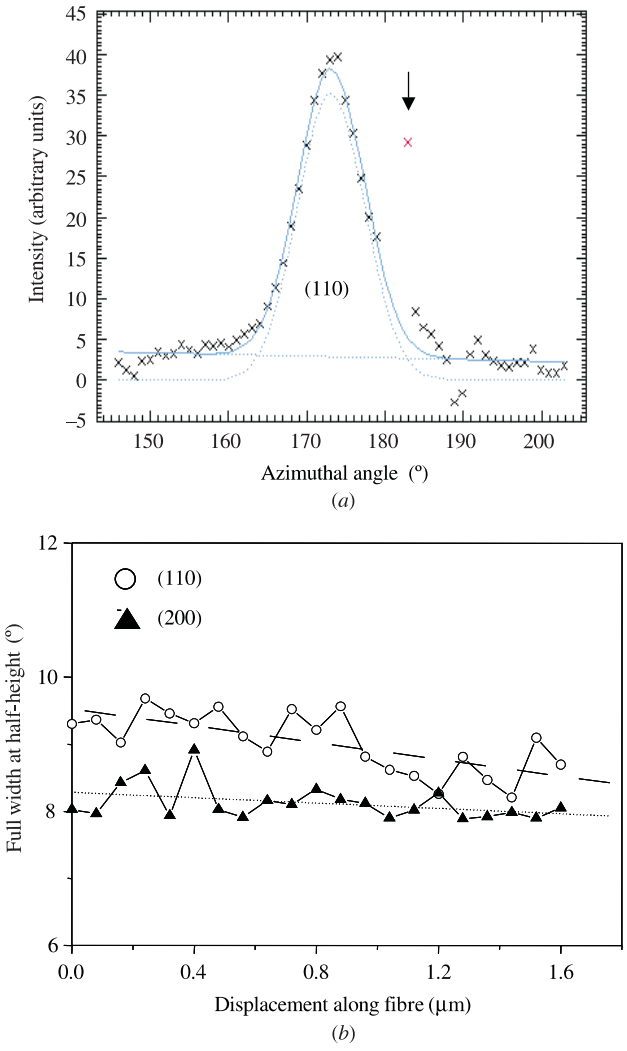

Figure 9
(*a*) Azimuthal intensity distribution of the Kevlar[49] 110 reflection in a single pattern. The intensity was radially averaged across the reflection profile. The peak marked by an arrow arises from the background and was masked during fitting of a Gaussian function and a first-order polynomial background (dotted lines). (*b*) Variation of the azimuthal width of the 110 and 200 reflections (Gaussian function; FWHM) during the linear scan. Lines correspond to least-squares fits to the data points.

more narrow reflection profiles as compared to the maxima. The period of modulation corresponds roughly to the expected 0.5 μm for the pleated-sheets model (Dobb *et al.*, 1977), although the modulation does not appear to be completely regular. It should, however, be noted that the pleated-sheet model is an idealized model and electron scattering experiments are usually performed on particularly well ordered thin slices. Experiments on whole fibres will, however, be sensitive to any deviation from perfect local order. It will be of interest to see whether this effect can also be observed in equatorial reflections from the fibre edge (Dobb *et al.*, 1977) and differently treated PPTA fibres. The scan along the central part of the fibre suggests, therefore, the presence of a single phase with a homogeneous particle size distribution, but with a possible slight modulation of crystallite orientation distribution.

4.4. Small-angle X-ray scattering (SAXS)

SAXS, although with limited resolution, should be possible in view of a divergence of about 1 mrad in the TE_0 mode. Furthermore, calculations suggest that the TE_0 mode should produce a more rapid decrease of the fringe pattern as compared to a classical slit with the same dimension (Cedola, 1998). Fig. 11(*a*) shows first the wide-angle scattering pattern (WAXS) obtained from a stretched poly(ethylene terephthalate) (PET) foil, of thickness 200 μm, with the present waveguide setup. The sample was again rotated by about $\Delta SR_x = 5°$. The pattern is identical to a pattern obtained with an $S = 10$ μm beam with a divergence of 2 mrad (horizontal) × 0.1 mrad (vertical) (Riekel, 2000) for a domain size of $L \simeq 10$ nm (Prevorsek *et al.*, 1977). The SAXS pattern obtained from the same PET sample and, for comparison, a SAXS pattern obtained with an $S = 10$ μm beam are shown in Fig. 11(*b*). The weak four-point pattern is also observed with the waveguide beam although the size and position of the beamstop were not optimized. A further reduction/optimization of background scattering has recently been obtained, allowing recording of both SAXS and WAXS. The effects of the fringe pattern (see above), which represents a limitation for weak scattering along the meridian, can be circumvented to a certain degree by a rotation of the sample around the beam direction (SR_x).

5. Conclusions and outlook

The use of waveguide optics offers the opportunity to approach the 0.1 μm beam size level in one dimension for diffraction experiments. Additional horizontal beam compression to about 3 μm FWHM has been made possible by the use of a multilayer mirror. The strong anisotropy of the beam suggests that the main applications will be in special geometry experiments on fibres or interfaces, which can be brought close to the waveguide exit. The modular setup developed has shown sufficient stability for extended scans at the 0.1 μm level. Further experiments are planned to explore its stability and possible modifications.

An extrapolation of the setup to the 2/3 filling mode with ≤200 mA ring current plus an optimized vacuum path at the beamline suggests that about 10^9 photons s^{-1} are feasible with the current undulator, of length 1.6 m and period 46 mm. This implies a flux density of $\leq 3 \times 10^7$ photons s^{-1} mA^{-1} μm^{-2}, which is only a factor of 3–4 less than that presently reached by composite optics composed of a condensing mirror and tapered glass capillary on ID13 (Riekel, 2000). Apart from a further increase in waveguide efficiency, the flux at the entrance of the waveguide could be increased in several ways. An undulator with a magnetic period such that the fundamental is at about 13 keV would result in an increase of flux by a factor of about 7 (P. Elleaume, personal communication). By increasing the distance of the waveguide to the source, one

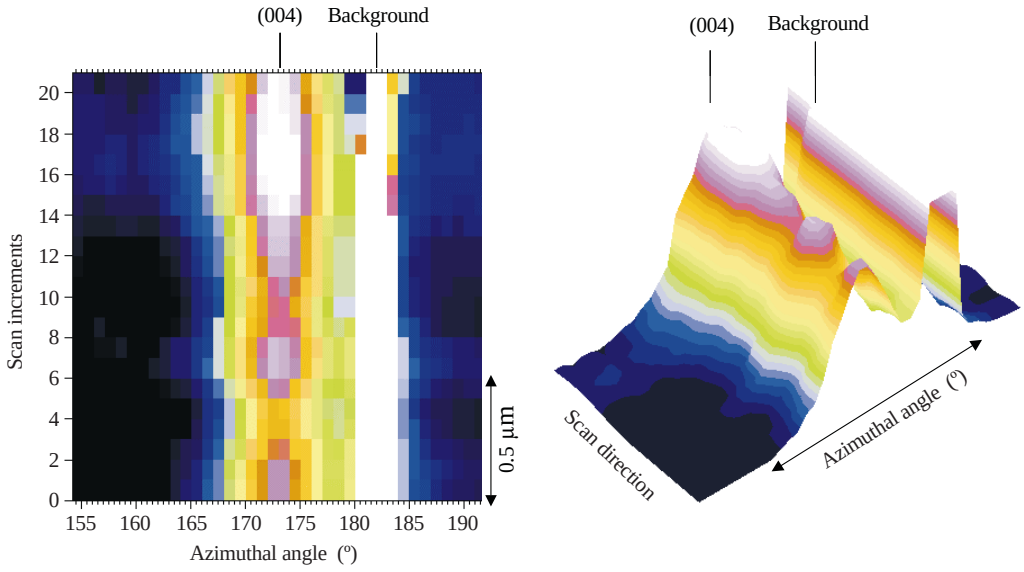

Figure 10
Variation of the azimuthal intensity of the Kevlar[49] 004 reflection during a linear scan along the fibre axis. The radial intensity distribution of the reflection has been averaged. (*a*) Projection onto the scanning axis. The period of the so-called pleated-sheet model (0.5 µm) is indicated. (*b*) Pseudo-three-dimensional plot.

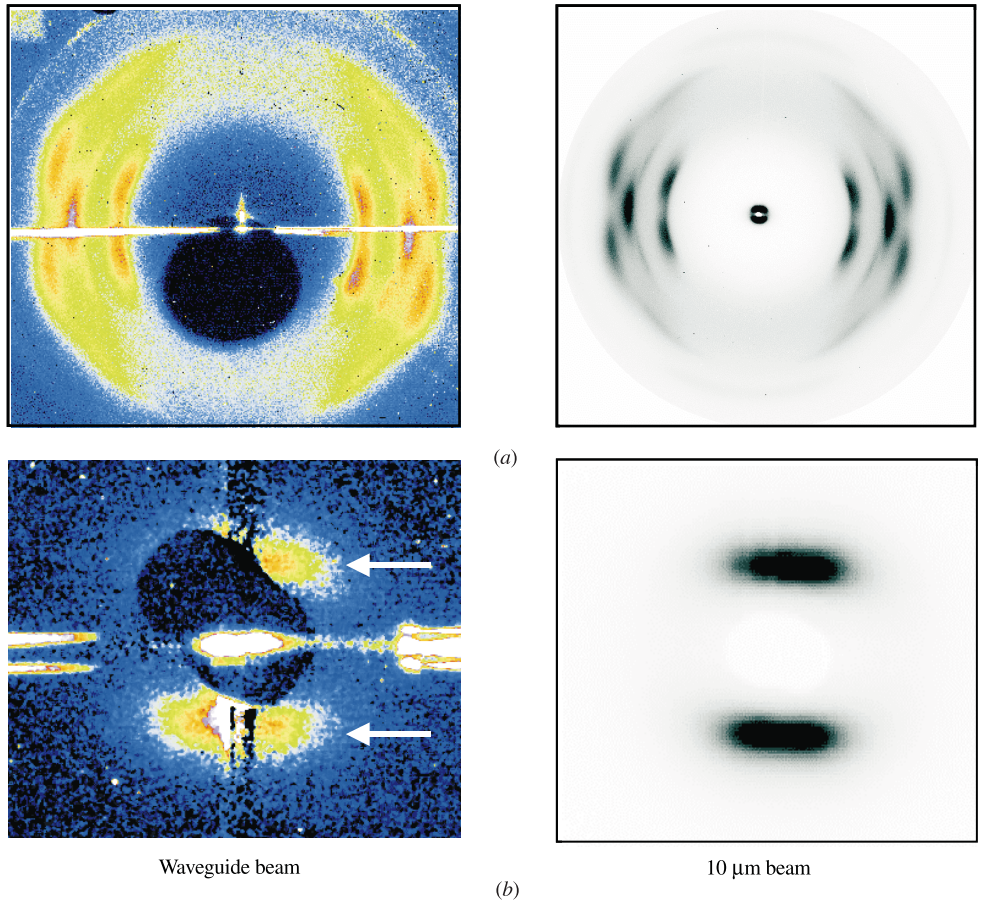

Figure 11
(*a*) WAXS pattern of a stretched PET foil recorded with a waveguide beam (left) and a 10 µm collimated beam (right); MAR CCD detector. (*b*) SAXS pattern of the same sample. Arrows indicate the position of the SAXS pattern. Waveguide-to-detector distance: 496.2 mm. Collimator-to-detector distance: ∼150 mm. The background has been subtracted in all cases. The SAXS pattern corresponds to a periodicity of about 10 nm.

could install a refocusing mirror with a demagnification of about 1:1 of the source onto the waveguide. Assuming a mirror reflectivity of about 0.5, this would increase the flux density at the entrance of the waveguide by a factor of about 16. In practice, one would probably choose a slightly larger spot at the waveguide in order to cope with beam instability effects.

The rather easy alignment and operation of the composite optics also suggests investigating horizontal submicrometre beam compression by a mirror.

We wish to thank E. Chinchio, O. Hignette and E. Ziegler for operational assistance during the alignment of the optics and the testing of the mirror. W. Jark and S. Lagomarsino made helpful suggestions concerning the use of the waveguide. E. Pantos provided the sample of the Koan amphora handle and assisted in the interpretation of the data. I. Snigireva recorded the SEM images.

References

Bilderback, D. H., Hoffman, S. A. & Thiel, D. J. (1994). *Science*, **263**, 201–203.
Cedola, A. (1998). PhD thesis, Physics Department, Joseph Fourier University, Grenoble.
Cedola, A., Lagomarsino, S., Di Fonzo, S., Jark, W., Riekel, C. & Deschamps, P. (1998). *J. Synchrotron Rad.* **5**, 17–22.
DiFonzo, S., Jark, W., Lagomarsino, S., Giannini, C., DeCaro, L., Cedola, A. & Mueller, M. (2000). *Nature (London)*, **403**, 638–640.
Dobb, M. G., Johnson, D. J. & Saville, B. P. (1977). *J. Polym. Sci. Polym. Phys. Ed.* **15**, 2201–2211.
Feng, Y. P., Sinha, S. K., Deckman, H. W., Hastings, J. B. & Siddons, D. P. (1995). *Appl. Phys. Lett.* **67**, 3647–3649.
Hignette, O., Freund, A. & Chinchio, E. (1997). *SPIE Proc.* **3152**, 188–199.
Iida, A. & Hirano, K. (1996). *NIM B*, **114**, 149–153.
Jackson, C. L., Schadt, R. J., Gardner, K. H., Chase, D. B., Allen, S. R., Gabara, V. & English, A. D. (1994). *Polymer*, **35**, 1123–1131.
Jark, W. *et al.* (2000). In preparation.
Jark, W., DiFonzo, S., Lagomarsino, S., Cedola, A., Di Fabrizio, E., Bram, A. & Riekel, C. (1996). *J. Appl. Phys.* **80**, 4831–4836.
Kuznetsov, S. M., Snigireva, I., Snigirev, A. A., Engström, P. & Riekel, C. (1994). *Appl. Phys. Lett.* **65**, 827–829.
Lagomarsino, S., Cedola, A., Cloetens, A. P., Di Fonzo, S., Jark, W., Soullié, G. & Riekel, C. (1997). *Appl. Phys. Lett.* **71**, 2557–2559.
Lai, B., Yun, W., Maser, J., Cai, Z., Rodrigues, W., Legnini, D., Chen, Z., Krasnoperova, A. A., Vladimirsky, Y., Cerrina, F., Di Fabrizio, E. & Gentili, M. (1998). *SPIE Proc.* **3449**, 133–136.
Morawe, C., Peffen, J. C., Gignette, O. & Ziegler, E. (1999). *SPIE Proc.* **3773**, 90–99.
Northolt, M. G. (1974). *Eur. Pol.* **10**, 799–804.
Padmore, H. A., Ackerman, G., Celestre, R., Chang, C. H., Franck, K., Howells, M., Hussain, Z., Irick, S., Locklin, S., MacDowell, A. A., Patel, J. R., Rah, S. Y., Renner, T. R. & Sandler, R. (1997). *Synchrotron Rad. News*, **10**(6), 18–26.
Prevorsek, D. C., Kwon, Y. D. & Sharma, R. K. (1977). *J. Mater. Sci.* **12**, 2310–2328.
Riekel, C. (2000). *Rep. Prog. Phys.* **63**, 233–262.
Riekel, C., Dieing, T., Engström, P., Vincze, L., Martin, C. & Mahendrasingam, A. (1999). *Macromolecules*, **32**, 7859–7865.
Sawyer, L. C. & Grubb, D. T. (1996). *Polymer Microscopy*. London: Chapman and Hall.
Snigirev, A., Kohn, V., Snigireva, I. & Lengeler, B. (1996). *Nature (London)*, **384**, 49–51.
Spiller, E. & Segmüller, A. (1974). *Appl. Phys. Lett.* **24**, 60–61.
Ziegler, E., Hignette, O., Lingham, M. & Souvorov, A. (1996). *SPIE Proc.* **2856**, 61–67.
Zwanenburg, M. J., Peters, J. F., Bongaerts, J. H. H., de Vries, S. A., Abernathy, D. L. & van der Veen, J. F. (1999). *PRL*, **82**(8), 1696–1699.